



## Divergent sensitivity of vegetation to aridity between drylands and humid regions

Guolong Zhang<sup>a,b</sup>, Yongli He<sup>b</sup>, Jianping Huang<sup>a,b,\*</sup>, Li Fu<sup>b</sup>, Dongliang Han<sup>a,b</sup>, Xiaodan Guan<sup>a,b</sup>, Beidou Zhang<sup>a,b</sup>

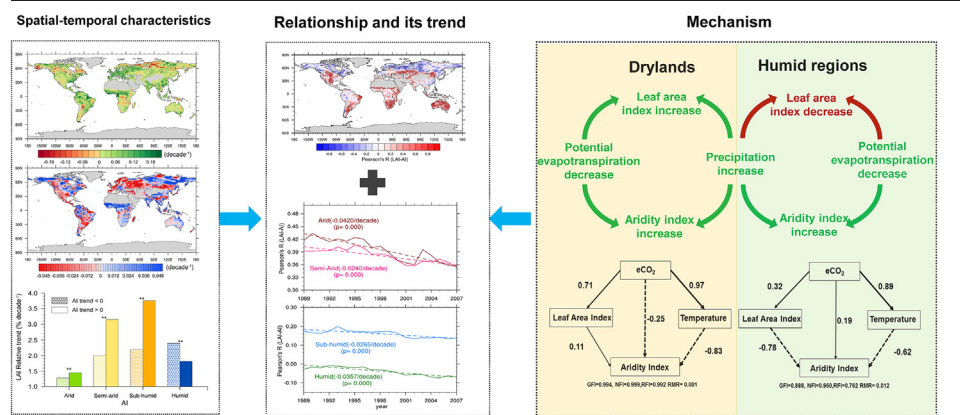
<sup>a</sup> Collaborative Innovation Center for Western Ecological Safety, Lanzhou University, Lanzhou 730000, China

<sup>b</sup> Key Laboratory for Semi-Arid Climate Change of the Ministry of Education, College of Atmospheric Sciences, Lanzhou University, Lanzhou 730000, China

### HIGHLIGHTS

- LAI increased significantly while AI increased slightly during past three decades.
- The response of LAI to AI is divergent across climatological region.
- The sensitivity of LAI to AI decreased in drylands and increased in humid regions.
- Increasing CO<sub>2</sub> resulted in decouple between LAI with AI in drylands.

### GRAPHICAL ABSTRACT



### ARTICLE INFO

Editor: Zhaozhong Feng

#### Keywords:

Leaf area index  
Aridity index  
Drylands expansion  
Global greening  
Effect of CO<sub>2</sub>

### ABSTRACT

The land surface has been drying over recent decades, which is inconsistent with the greening of the Earth. The extent and spatial variation in the sensitivity of vegetation to aridity changes in drylands and humid regions remain unclear. In this study, satellite observation and reanalysis data were used to analyze the relationship between vegetation growth and atmospheric aridity changes in different climatological regions on a global scale. Our results showed that the leaf area index (LAI) increased at a rate of 0.032/decade from 1982 to 2014, while the aridity index (AI) increased slightly at a rate of 0.005/decade. Over the past three decades, the sensitivity of the LAI to AI has decreased in drylands and increased in humid regions. Thus, the LAI and AI were decoupled in drylands, whereas the effect of aridity on vegetation was enhanced in humid regions during the study period. The physical and physiological effects of increasing CO<sub>2</sub> concentration are responsible for the divergent responses of vegetation sensitivity to aridity in drylands and humid regions. The results of the structural equation models showed that the effect of increasing CO<sub>2</sub> concentration via LAI and temperature, with respect to decreasing AI, enhanced the negative relationship between LAI and AI in humid regions. The greenhouse effect of increasing CO<sub>2</sub> concentration resulted in an increase in temperature and a reduction in aridity, whereas the fertilization effect of CO<sub>2</sub> increased LAI, thus creating an inconsistent trend with LAI and AI in drylands.

\* Corresponding author at: Collaborative innovation center for western ecological safety, Lanzhou University, Lanzhou 730000, China.  
E-mail address: [hjp@lzu.edu.cn](mailto:hjp@lzu.edu.cn) (J. Huang).

## 1. Introduction

Changes in water availability on land are key drivers of the impacts of climate change on human and natural systems (Berg et al., 2016). Aridity index (AI), the ratio of annual precipitation (P) to annual potential evapotranspiration (PET), is widely used to describe the scarcity of the water supply relative to the atmospheric demand for moisture (Huang et al., 2017a, b); it is also used to define global dryland areas (IPCC, 2019). Observations and model results indicate that much of the land has been drying (Huang et al., 2016a,b), which corresponds to a decrease in AI. With global warming, the Earth will face a warmer and drier future (Sherwood and Fu, 2014). Drylands are expected to expand (Feng and Fu, 2013; Huang et al., 2016b, 2017a,b), thereby increasing the risk of desertification in the future (Huang et al., 2012, 2020). Aridity has a significant effect on the structure and function of dryland ecosystems (Berdugo et al., 2020). As aridity increases, the cycles of carbon, nitrogen, and phosphorus would decouple in drylands, which negatively affects the key processes in these ecosystems (Delgado-Baquerizo et al., 2013) and triggers increased tree mortality (Kharuk et al., 2013). Numerous studies have shown that grasslands and forest ecosystems have been influenced by increasing aridity, such as the Tibetan Alpine Grasslands (Ding et al., 2018), the Greater Yellowstone Ecosystem in the Northern Rocky Mountains (Brookshire and Weaver, 2015), and the grasslands of the United States (Konings et al., 2017). Eurasian boreal forest greening has also shifted (Buermann et al., 2014), and the global net primary production has decreased over the past decade (Zhao and Running, 2010).

At the same time, however, the globe has experienced 'greening' over the past three decades (De Jong et al., 2012; Fensholt et al., 2012; Piao et al., 2020), based on a body of work including in situ and satellite observation evidence. Long-term changes in vegetation greenness are influenced by many factors, including the fertilization effect of increasing atmospheric CO<sub>2</sub> concentration (eCO<sub>2</sub>), nitrogen deposition, climate change, and human activity (Zhu et al., 2016). eCO<sub>2</sub> can enhance photosynthesis by accelerating the rate of carboxylation and increase vegetation greenness by improving water-use efficiency (Piao et al., 2020). eCO<sub>2</sub> has proven to be the dominant factor in global greening, as demonstrated by observational data and model results, particularly in drylands (Lu et al., 2016; Donohue et al., 2013; Zhu et al., 2016). Climate change is another important driver of greenness variation. He et al. (2019) reported that increasing precipitation is the main driver of greening over drylands. Human activities also significantly influence land cover through deforestation, afforestation, and agricultural activities. Song et al. (2018) reported that human activity accounted for 60 % of the changes in global land type from 1982 to 2016. Chen et al. (2019) pointed out that greening patterns have been strikingly prominent in China and India since 2000 and have overlapped with crop-lands worldwide.

Several studies have attempted to reconcile the paradoxes of global greening and drying. Based on the analyses of meteorological, hydrological, and agroecological aridity, Roderick et al. (2015) concluded that warmer conditions coincide with less arid conditions. Previous studies have revealed the fertilization effect of eCO<sub>2</sub> on the vegetation, while other studies have pointed out overestimated PET due to decreasing stomatal conductance (Berg et al., 2016; Yang et al., 2019). So those studies have implied that the relationship between leaf area index (LAI) and AI has changed due to eCO<sub>2</sub> and climate change; however, the relationship between changes in AI and LAI varies spatially and remains to be fully understood. Additionally, the extent to which this relationship changes remain unclear. This hampers our ability to understand vegetation change and its responses to climate change, and results in contradictory conclusions about future dryland expansion (Huang et al., 2016b; Berg and McColl, 2021). In this study, we used three decades of LAI and AI observations to investigate their relationship across various climatological regions at a global scale. We evaluated the long-term trends of the relationship between vegetation greenness and aridity change across different climatological regions. The mechanisms underlying the changing sensitivity of vegetation to aridity due to eCO<sub>2</sub> was also investigated. Our study is crucial for understanding

the response of vegetation to the aridity change in the different climatological regions, and for improving future projections of vegetation dynamics under a changing climate.

## 2. Materials and methods

### 2.1. Datasets

#### 2.1.1. Satellite datasets

LAI is a key biophysical parameter for the monitoring of agroecosystems, which was widely used to the global change and ecological studies (Zhu et al., 2016; Piao et al., 2020). In this study the satellite-observed LAI products (GIMMS LAI3g) are used to analyze the changes in global vegetation for the period 1982–2014. The GIMMS is currently considered the best dataset in overcoming data inconsistencies resulting from the utilization of multiple satellite sensor systems. The GIMMS LAI3g dataset was derived from the Advanced Very High Resolution Radiometer after sensor calibration, volcanic aerosols, and other sensor degradation and contamination issues and is available at 8 km horizontal resolution every 15 days (Zhu et al., 2013). When we tested trends in LAI at global and continental scales, we calculated the mean of LAI values of all the pixels in the specific region, weighting by  $\cos(\theta_i/\pi/180.0)$ , here  $\theta_i$  is the latitude of the grid  $i$ .

#### 2.1.2. Climate datasets

The AI represents how well the water supply can meet the demand, is defined as the ratio of annual P to annual PET, and is computed as:

$$AI = \frac{P}{PET} \quad (1)$$

Under this quantitative indicator, humid regions are defined as  $AI \geq 0.65$ , while drylands are regions where  $AI < 0.65$  and are further divided into subtypes of hyper-arid ( $AI < 0.05$ ), arid ( $0.05 \leq AI < 0.2$ ), semi-arid ( $0.2 \leq AI < 0.5$ ), and sub-humid ( $0.5 \leq AI < 0.65$ ) regions. Herein, climatological AI is the mean of annual AI for the period 1961–1990 (Feng and Fu, 2013; Huang et al., 2016a,b). The precipitation data is from the NOAA's PRECipitation REConstruction over Land (PREC/L) dataset developed by the Climatic Prediction Center (CPC), which was interpolated from station data from the Global Historical Climatology Network (GHCN) version 2 and Climate Anomaly Monitoring System (CAMS) dataset with a spatial resolution of 0.5° for 1948 to the present. The PET and temperature data were retrieved from CRU TS 3.25 dataset (Harris et al., 2014) with a spatial resolution of 0.5° for 1901–2014.

#### 2.1.3. CO<sub>2</sub> datasets

Here, we used the global annual CO<sub>2</sub> data obtained from the Global Monitoring Laboratory of NOAA for 1980–2021. The global mean surface values using measurements of weekly air samples from the Cooperative Global Air Sampling Network (Conway et al., 1994; Trolier et al., 1996) and a global average was calculated from the latitude plot at each time step (Masarie and Tans, 1995).

All the datasets were aggregated to 0.5°. As the LAI is not available in some barren areas, to maintain consistency with the LAI, we masked the region where the value of the LAI was missing when we calculated the AI mean and trend in this study.

## 2.2. Methods

### 2.2.1. Statistical method

The Pearson correlation was performed between annual LAI and AI over the period 1982–2014. We also investigated the trend of relationship between annual LAI and AI over the period 1982–2014 by the 15-years moving windows. The Theil–Sen trend analysis, which is a linear trend calculation that is resistant to the impact of outliers (noise) was used to quantify the LAI and AI trend. The Mann–Kendall (MK) method was used to test the significance of trend. A value of +1 indicates a trend that

continuously increases and a value of  $-1$  if it always decreases. A value of 0 indicates no consistent trend.

The assessment of the relationship between the LAI and AI requires the analysis of the temporal fluctuation of these variables. The temporal variability of these quantities was affected by long-term trends of drivers like temperature,  $e\text{CO}_2$ , nitrogen deposition, etc. In order to filter out the effect of the trends in the covariates, we based the analysis on interannual variations of LAI and AI across AI gradient following Forzieri et al. (2017).

### 2.2.2. Multidimensional ensemble empirical mode decomposition

We used multidimensional ensemble empirical mode decomposition (MEEMD) to investigate the trend of LAI and AI. MEEMD is a way to separate spatiotemporally varying trends and spatially nonuniform variability of different time scales based on EEMD (Huang et al., 1998; Wu and Huang, 2009). In MEEMD, a time series was decomposed to a set of intrinsic mode functions (IMFs) based on EEMD at each grid pixel, which are a series of amplitude frequency-modulated oscillatory components. The last IMF is recognized as the trend of the time series, which is sensitivity to the

extension (addition) of new data. MEEMD has been widely applied in climate research (Ji et al., 2014; Wu et al., 2011). In this study, we choose that ensemble number is 400; the number of IMFs is 5 and added the noise to data has an amplitude of 0.2 standard deviations of the corresponding data following Cheng et al. (2015).

### 2.2.3. The contribution of different region

Contribution is one of the important factors to justify the local change extent to global change (Huang et al., 2012), which can reflect the role of regional aridity and vegetation change to their global change. Here, we calculated the contribution rate ( $CR_k$ ) of region  $k$  as:

$$CR_k = \frac{a_k \cdot \sum_{i=1}^{N_k} W_{ki}}{A_g \cdot \sum_{i=1}^{N_g} W_i} \quad (2)$$

where  $a_k$  is the trend of mean AI or LAI for region  $k$ ,  $A_g$  is the trend of the global mean AI or LAI,  $N_k$  is the number of grids in region  $k$ , and  $N_g$  is the

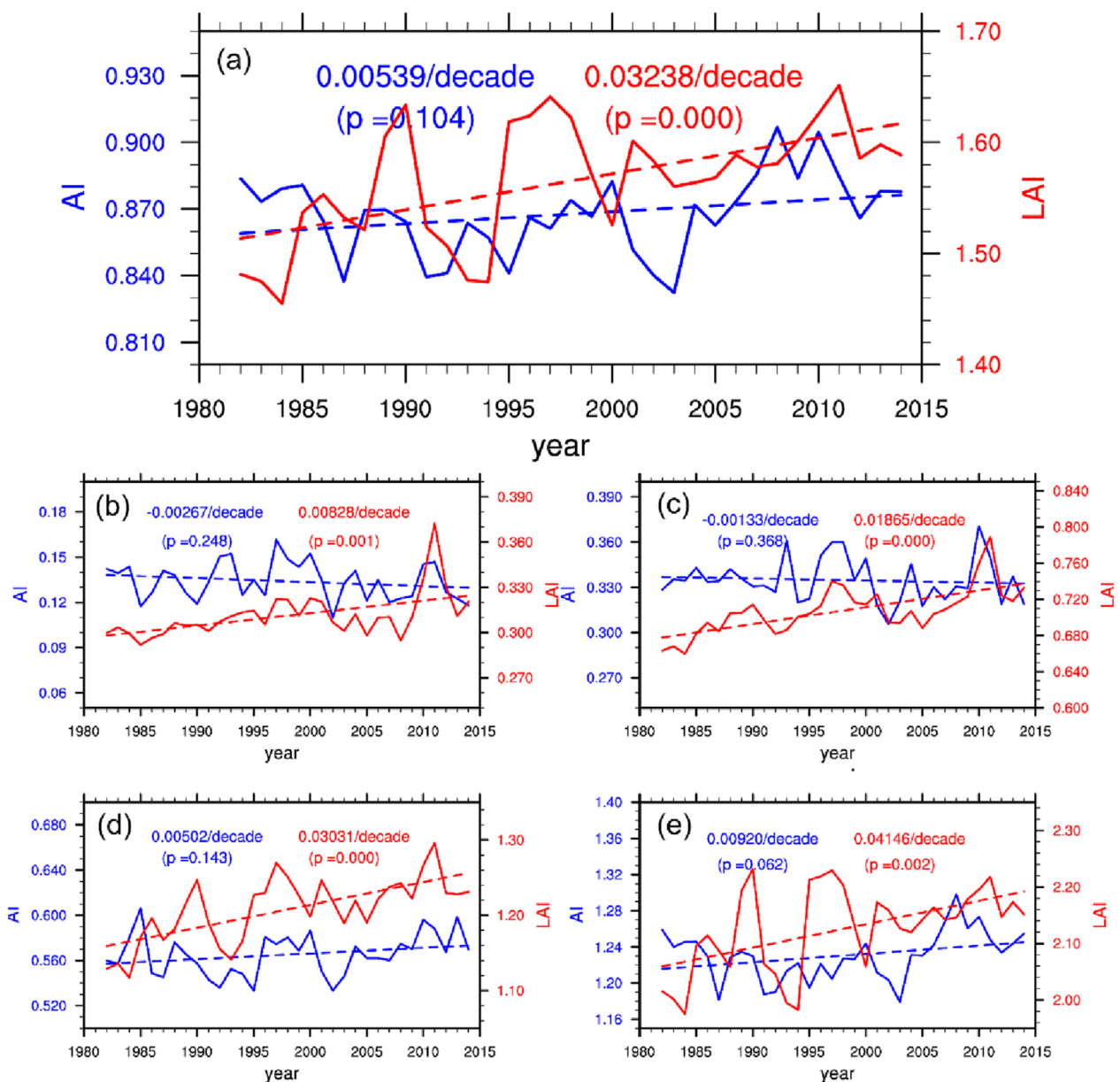


Fig. 1. The time series of annual leaf area index (LAI) and aridity index (AI) from 1982 to 2014 in (a) global, (b) arid, (c) semi-arid, (d) sub-humid, and (e) humid regions. (The evolution in hyper-arid regions is not shown owing to small LAI; the red lines present LAI and the blue lines present AI. The Y-axis scales in the five subplots are different.)

total number of grids over global land.  $W_{ki}$  and  $W_i$  are the weighted factor of the grid  $i$ ,  $W_{ki} = \cos(\theta_{ki} \cdot \pi)/180.0$ ,  $\theta_{ki}$  is the latitude of the grid  $i$  in the region  $k$ ,  $W_i = \cos(\theta_i \cdot \pi)/180.0$ , and  $\theta_i$  is the latitude of the grid  $i$  in the region  $k$ .

#### 2.2.4. Structural equation model

The structural equation model (SEM) provides a statistical framework to deal with the complex relationships among different drivers, giving us a more comprehensive picture of their relative importance and providing insights into the mechanisms behind their effects (Grace, 2006; Maestre et al., 2016). In this study, the SEM was used to analyze the influence  $eCO_2$  on the relationship of LAI and AI in different climatological regions. The SEM analyses were performed using the AMOS 17.0 (IBM., Chicago, IL, USA).

### 3. Results

#### 3.1. Changes in LAI and AI

The global LAI increased at a rate of 0.032/decade and the AI increased at a rate of 0.005/decade from 1982 to 2014 (Fig. 1a). Thus, the Earth has become slightly wetter over the past three decades and the climate has become more favorable for vegetation growth. However, the AI decreased in arid and semi-arid regions at  $-0.003/\text{decade}$  and  $-0.001/\text{decade}$ , respectively, whereas the LAI showed an increasing trend (0.008/decade and 0.019/decade). Both LAI and AI increased in the sub-humid and humid regions (Fig. 1d, e). The trends of AI and LAI were not uniform at the global scale (Fig. 2). Increasing LAI has occurred mainly in the Northern

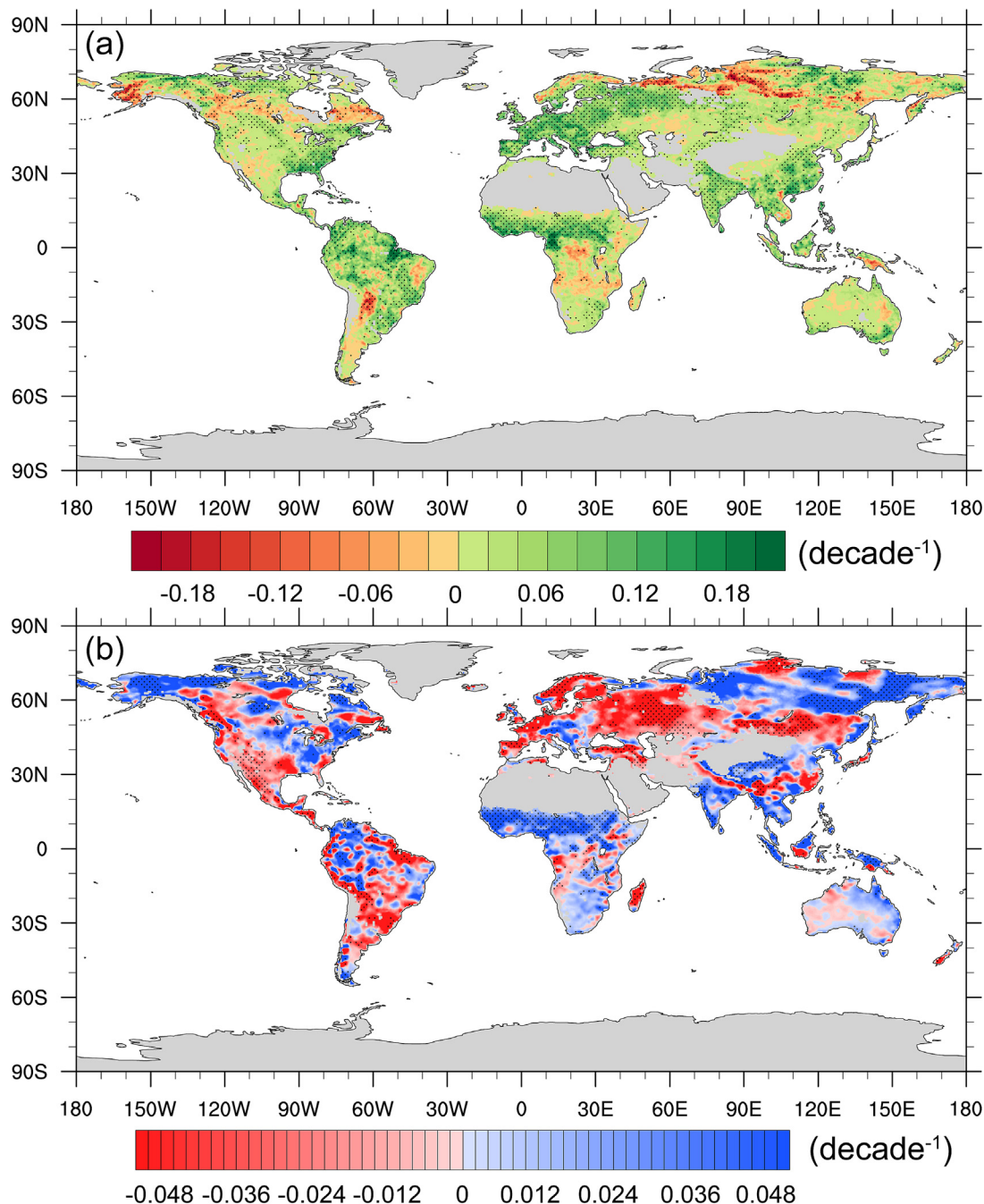


Fig. 2. The global distribution of linear trends of the (a) annual leaf area index (LAI) and (b) aridity index (AI) from 1982 to 2014. (The stippling represents significant trends at  $P < 0.05$ .)

Hemisphere over the past three decades, especially in Europe, Central Africa, Southeast North America, and Southeast Asia (Fig. 2a). AI increased significantly in Central Africa, India, Northeast North America, and South Africa (Fig. 2b).

The LAI trends in Europe, India, East China, Central Africa, and South America were the main contributors to the global annual LAI mean trend; however, the contribution of the LAI in the high latitudes was negative (Fig. 3a). As shown in Fig. 3b, the global trend of the area contributions to LAI change has a narrow distribution (mean = 0.002, SD = 0.004), but is skewed positively (skewness = 0.90), which indicates that the global trend for the annual LAI mean was dominated by limited concentration areas. The areas where the AI increased were mainly located in Central Africa and India, with the highest contributions being from the Tibetan Plateau, India, and Africa (Fig. 3c). Compared to the frequency of contributions for LAI, that of AI showed a larger standard deviation (mean = 0.0024, SD = 0.03) (Fig. 3d), which is consistent with the high spatial heterogeneity of the regional trend contribution to the global trend for the annual AI mean.

### 3.2. LAI changes in different climatological regions

Fig. 4 shows the LAI trends for different climatological regions from 1982 to 2014. It is worth noting that the LAI trend was greater under a positive AI trend than under a negative AI trend in drylands; conversely, the LAI trend was smaller under a positive AI trend than under a negative AI trend in humid regions (Fig. 4a). The trend was positive despite the changing AI type, suggesting that aridity change is not the dominant factor

driving the changing annual LAI in drylands or humid regions (Fig. 4b). There were two peaks in the trend of LAI, with respect to the climatological mean AI (Fig. 4c), located in the regions where the climatological AI ranged from 0.9 to 1.2 and from 1.6 to 1.9. The relative LAI trend, which is the ratio of trend LAI to the averaged LAI during 1982–2014, in the drylands was higher than that in humid regions (Fig. 4d).

Fig. 5 shows the contributions of the LAI and AI trends in different climatological regions to the global trend for annual means. The regions where the climatological AI ranged from 0.6 to 0.9 play a dominant role in the global annual AI trend. The regions where the climatological AI ranged from 0.9 to 1.2 play a key role in the global annual LAI trend, indicating that humid regions made the biggest contribution to global greening. As implied by the evolution of LAI based on the MEEMD, three LAI peaks were located in regions where the climatological AI ranged from 0.4 to 0.7, 0.9 to 1.2, and 1.6 to 1.9, in agreement with the results based on the linear trend, which are also important regions to global annual LAI trends.

### 3.3. Correlation between the LAI and AI

We further investigated the correlation between LAI and AI in different regions (Fig. 6). The regions with a positive correlation between LAI and AI were mainly located in Australia, Southern Africa, Central Asia, Northern China, and Central and Western America. Regions with a negative correlation between the LAI and AI were mostly located in the high latitudes of the Northern Hemisphere, particularly in Siberia (Fig. 6a). As the AI increased, the correlation increased until the AI approached 0.25, at which point the correlation decreased; when the AI crossed 0.80, there was a negative

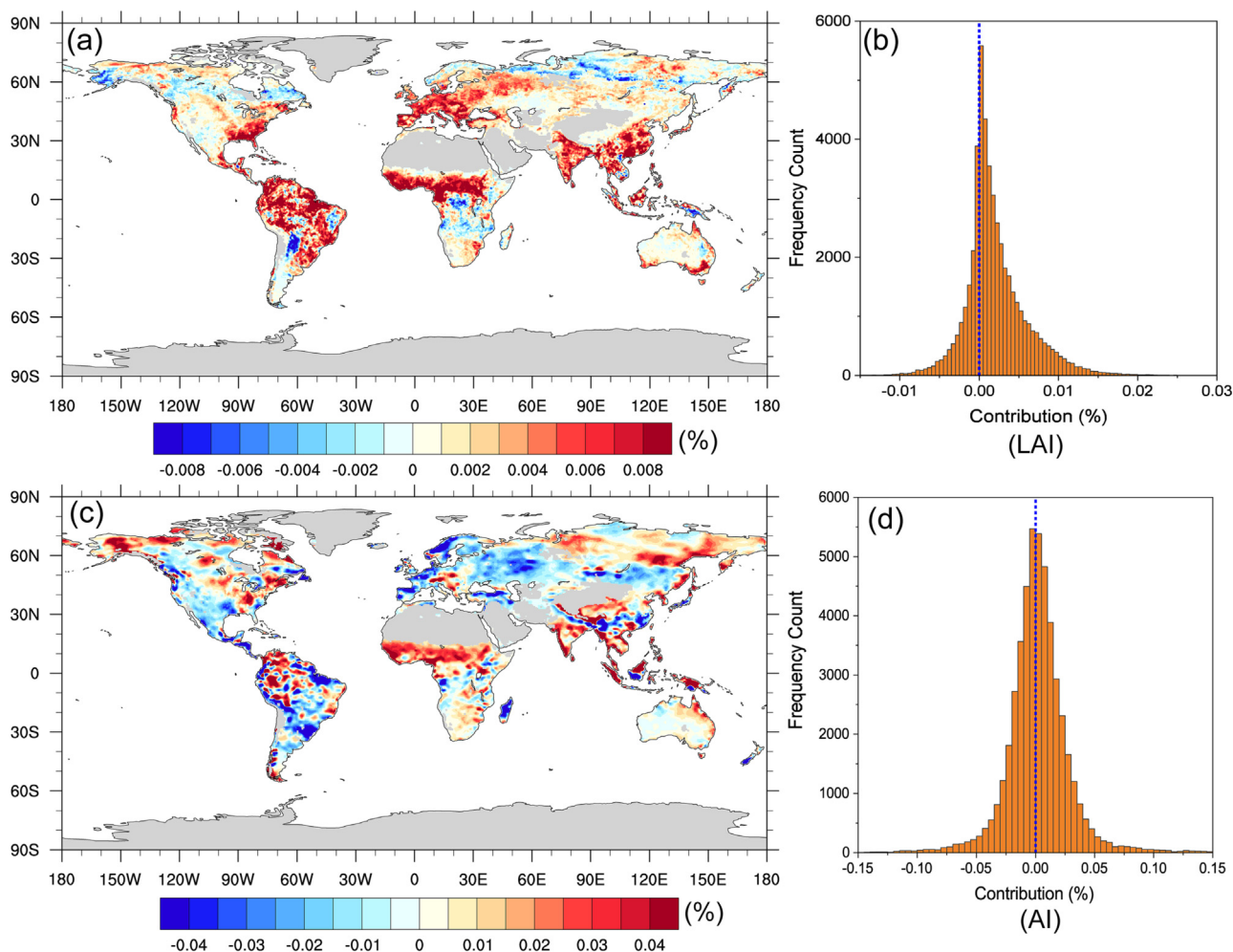


Fig. 3. The global distribution of the contribution rate of regional changes to the global leaf area index (LAI) change (a) and aridity index (AI) change (c); frequency distribution of the contribution rate of the regional LAI (b) and AI change (d).

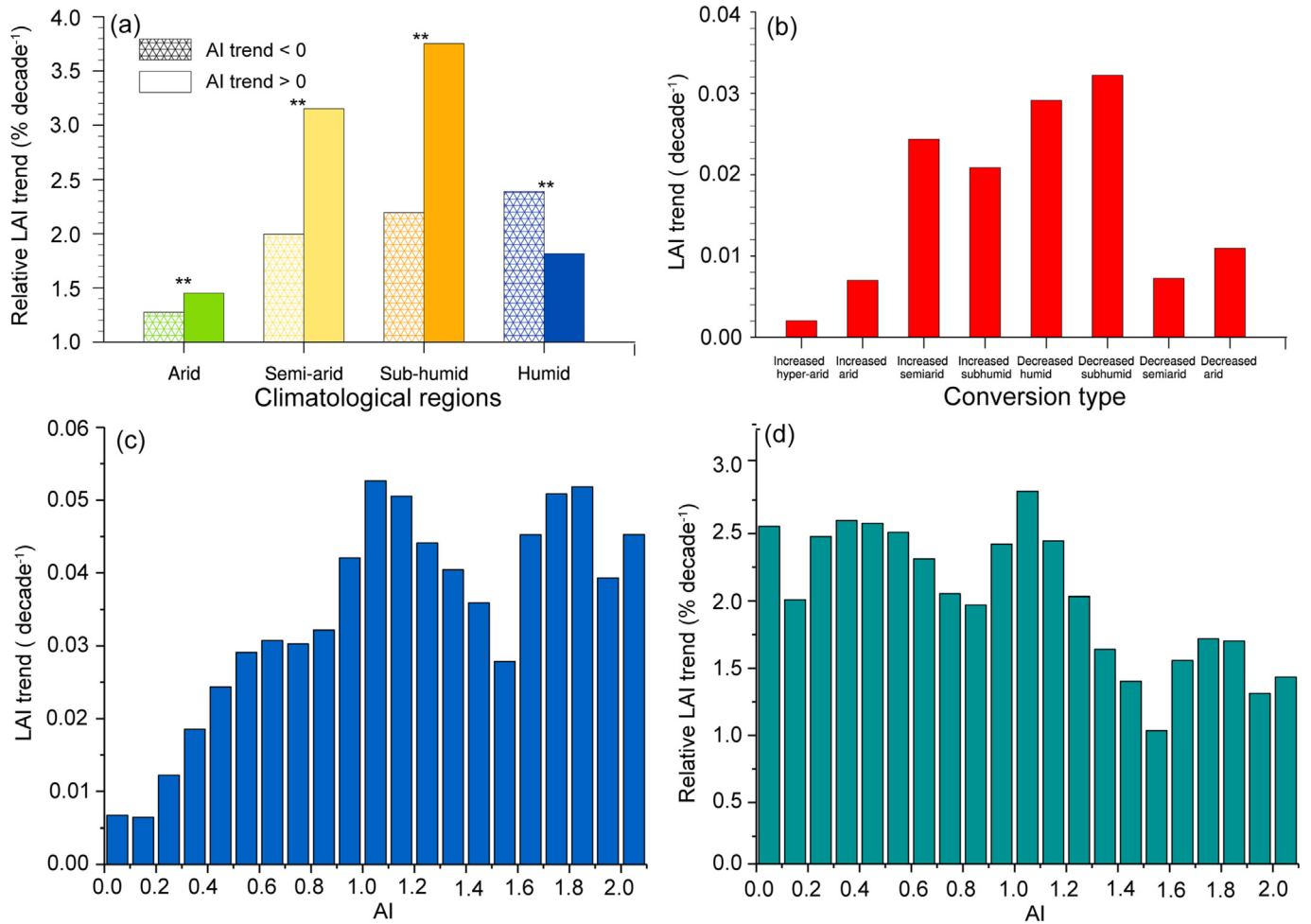


Fig. 4. The trend of leaf area index (LAI) under different climatological region (a) and under different conversion types (b), the linear trends of LAI (c) and relative LAI trend (d) during 1982–2014 as a function of the climatological mean AI. (\*\* represents a significant difference at  $P < 0.01$  based on a  $t$ -test in (a); the conversion includes any transition from adjacent and nonadjacent subtypes. The ‘increased’ category means the transitions from wetter to drier subtypes; the ‘decreased’ category refers to transitions from drier to wetter subtypes in (b). AI >2.2 are included in the last bar to the far right of plot in (c) and (d).)

relationship between LAI and AI (Fig. 6b). Therefore, considering the positive correlation between LAI and AI in drylands and the negative correlation in humid areas, a reduction in the global mean AI does not necessarily indicate a reduction in LAI. Fig. 6c shows the trend in the

correlation between LAI and AI over the past three decades using a 15-year moving-window analysis. The global distribution of the trend of correlation between LAI and AI showed high spatial heterogeneity, dominated by a negative trend. Regions with a negative trend of correlation were

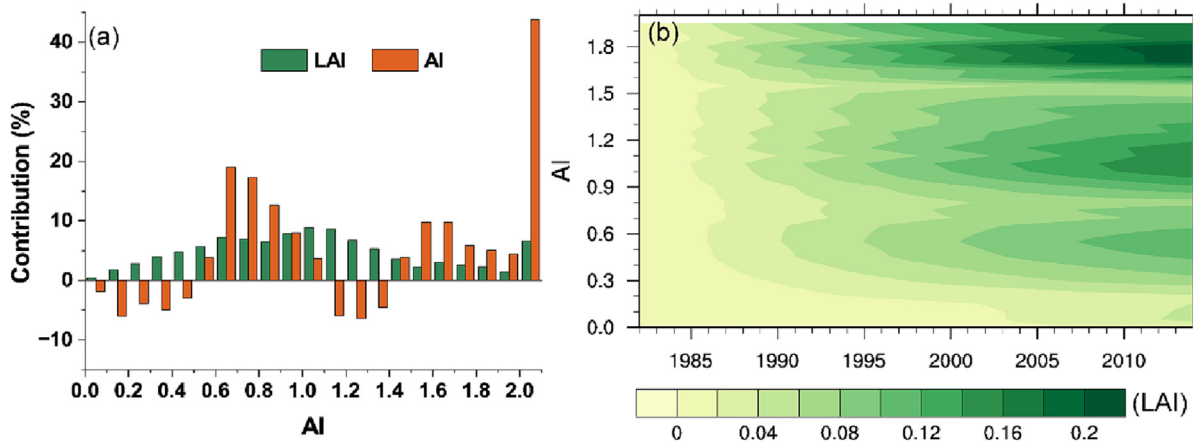
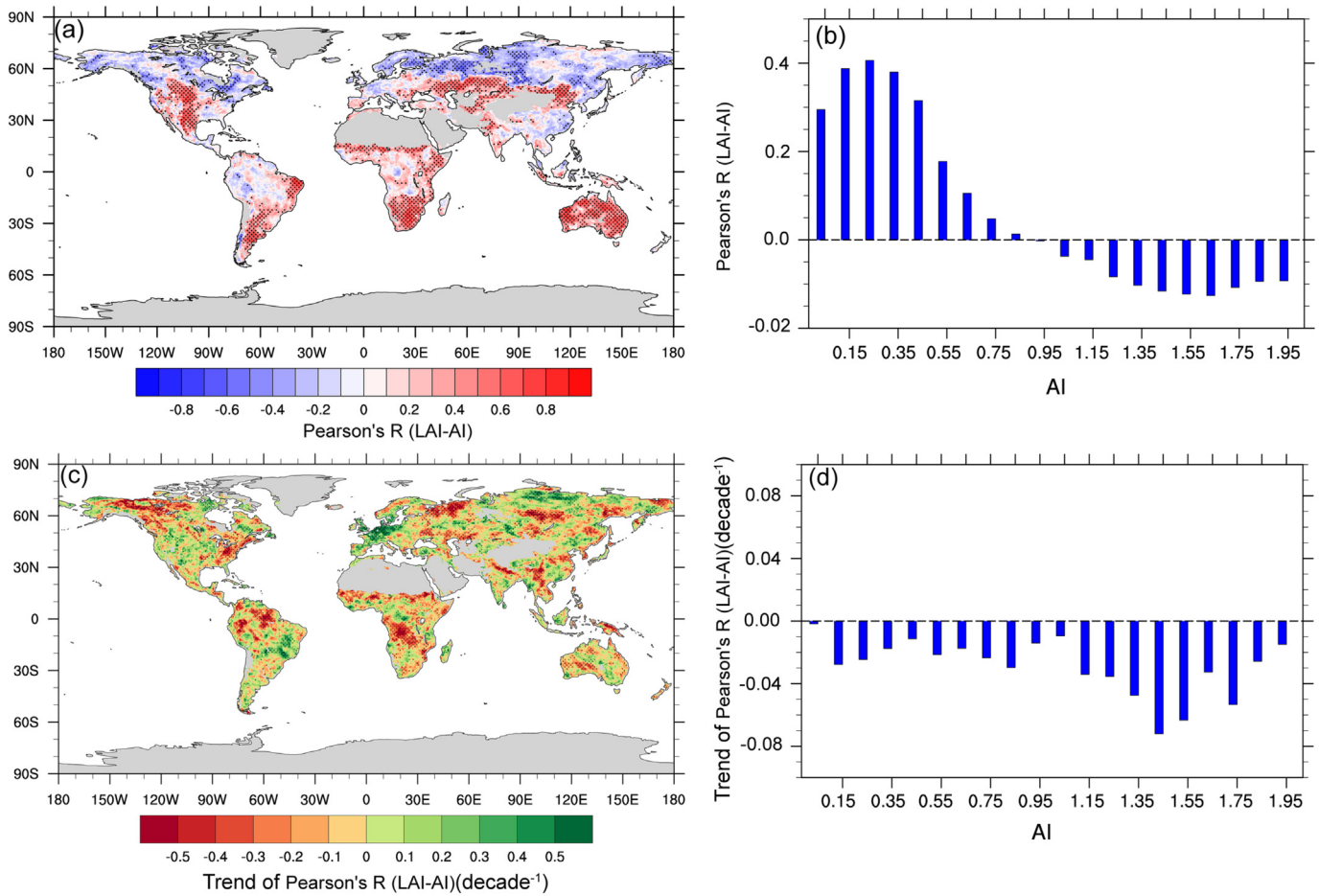


Fig. 5. The contribution of different climatological regions to the global aridity index (AI) and leaf area index (LAI) trend (a) and the evolution of the LAI trend (b) as a function of the climatological mean AI from 1982 to 2014 based on MEEMD. (The LAI contribution is presented as a green bar, while the AI contribution is presented as an orange bar.)



**Fig. 6.** The global distribution of the correlation (a) and trend of the correlation (c) between the LAI and AI from 1982 to 2014; the correlation (b) and the trend of correlation (d) between LAI and AI as a function of the climatological mean AI. (The stippling represents a significant correlation and trend at  $P < 0.05$  in (a) and (c), respectively.)

located in North Sahel, Central and Southern Africa, the Mediterranean, Eastern America, and Southwest China. Regions showing a positive trend of correlation included Europe, Brazil, and Central America (Fig. 6c). In the region where the AI value ranged from 1.4 to 1.6, the trend of the correlation value reached its maximum value (Fig. 6d). The trends of correlation values between LAI and AI over arid, semi-arid, sub-humid, and humid regions were  $-0.04$ ,  $-0.02$ ,  $-0.03$ , and  $-0.04/\text{decade}$ , respectively (Fig. 7). A reduction in the correlation value indicates that the relationship between LAI and AI decoupled in drylands over the three decades. However, the relationship between LAI and AI was stronger in humid regions, indicating a closer negative relationship between vegetation and aridity.

### 3.4. Mechanism underlying changes in LAI sensitivity to AI

Here, we analyzed annual variations in LAI and AI across the AI gradient, following Forzieri et al. (2017), to explain the different correlations between LAI and AI in different climatological regions. In dryland regions, the decreased AI coincided with a reduction in the LAI, in line with the positive correlation between the LAI and AI; however, in humid regions, the decreased AI was accompanied by an increased LAI, resulting in a negative correlation between the LAI and AI (Fig. 8e). To further explore the mechanism of the correlation between LAI and AI in different climatological regions over the past three decades, we examined the covariation effect of P and PET influence on LAI and AI in different climatological regions

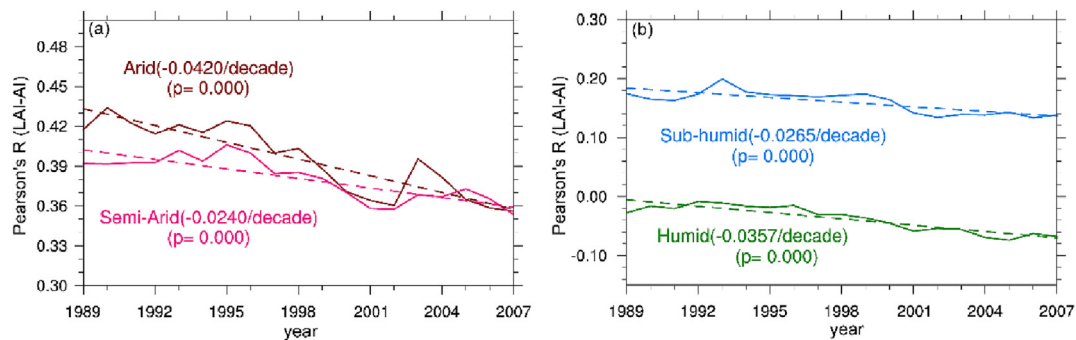


**Fig. 7.** The time series of the correlation between leaf area index (LAI) and aridity index (AI) during 1982–2014 with a fifteen-year moving-window in different climatological regions.

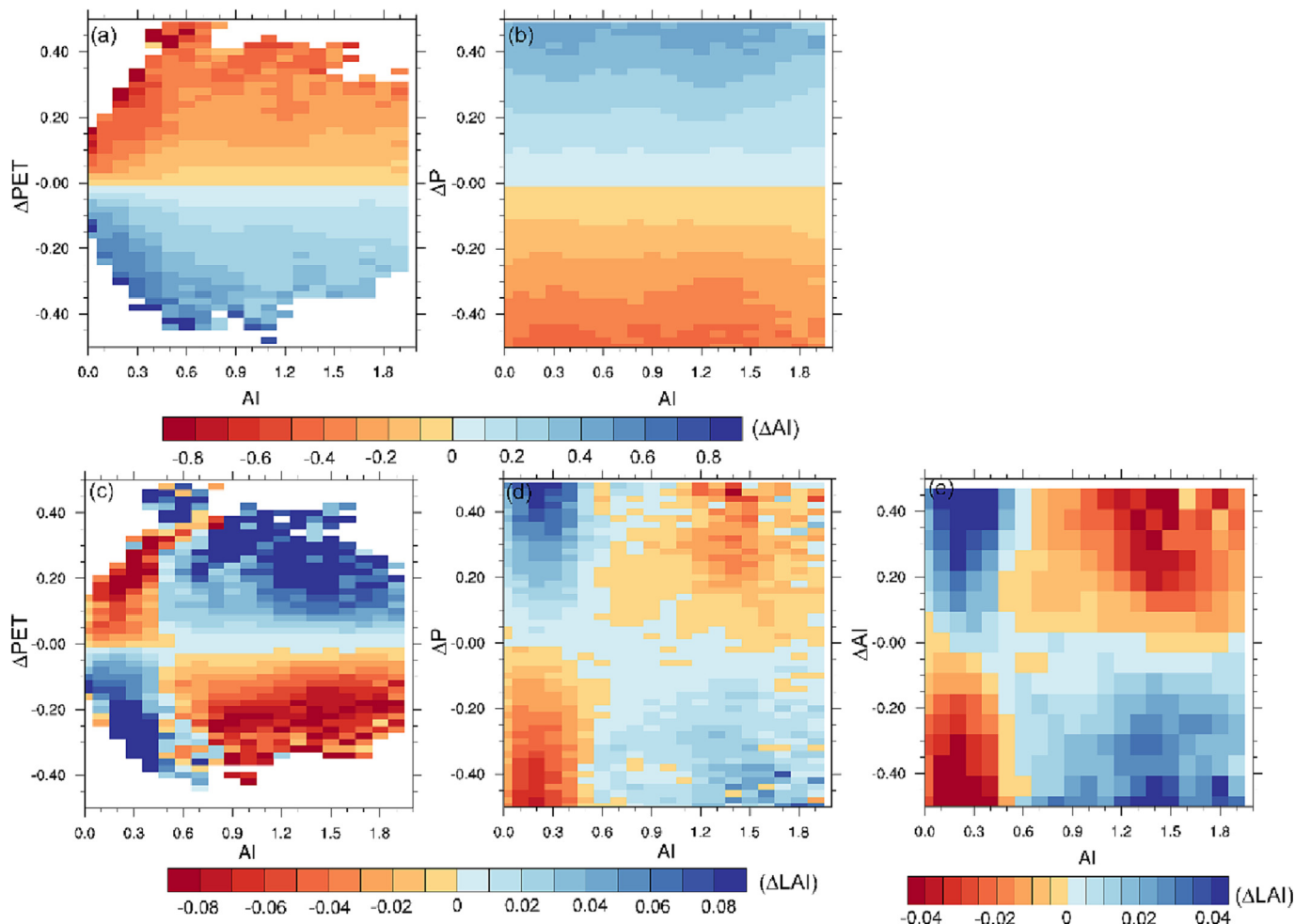


**Fig. 8.** Relative interannual variations of leaf area index (LAI, a) and aridity index (AI, c) against the relative interannual variations in potential evapotranspiration (PET, y axis) and the climatological mean AI. Relative interannual variations of LAI (b) and AI (d) against the relative interannual variations in precipitation (P, y axis) and the climatological mean AI. Relative interannual variations of LAI (e) against the relative interannual variations in AI (y axis) and the climatological mean AI.

(Fig. 8a-d). Increasing P and decreasing PET coincided with increasing AI in both the dryland and humid regions (Fig. 8a and b). However, the change in LAI depended on the climatological region. In drylands, increasing P and decreasing PET caused an increase in the LAI. In humid regions, increasing P and decreasing PET were accompanied by a reduction in the LAI (Fig. 8c and d). Thus, the consistent influence of P and PET on the AI and the contrasting effect on the LAI in dryland and humid regions resulted in a different correlation between the LAI and AI across climatological regions (Fig. 8e).

We further explored the effect of  $\text{eCO}_2$  on the trend of correlation between LAI and AI over the past three decades. The fertilization effect of  $\text{eCO}_2$  had a dominant effect on the increase in LAI over the past three decades. Vegetation plays a vital role in water and energy exchange between the land and atmosphere; thus, AI could be influenced by  $\text{eCO}_2$  through vegetation.  $\text{eCO}_2$  increases the temperature, which also influences the AI by increasing PET. Therefore, we hypothesized that  $\text{eCO}_2$  indirectly influenced AI via vegetation and temperature, and affected the relationship between LAI and AI. Based on this hypothesis, structural equation models were built for drylands and humid regions (Fig. 9). The results indicated that the direct effect of  $\text{eCO}_2$  on the AI was negative in drylands and positive in humid regions, the effect of  $\text{eCO}_2$  on AI through temperature was higher in drylands than in humid regions, and the effect of  $\text{eCO}_2$  on AI by LAI was positive in drylands and negative in humid regions. Ultimately, this resulted in the decoupling of the relationship between the LAI and AI in drylands; however, the effect of  $\text{eCO}_2$  via the LAI and temperature with

respect to a decreasing AI enhanced the relationship between the LAI and AI in humid regions.

#### 4. Discussion

Our results revealed that the LAI increased globally, which is in line with previous studies (Zhu et al., 2016). AI decreased in the arid and semi-arid regions (Fig. 1), while the relative LAI trend was largest (Fig. 4d), that mainly due to the fertilization effect of  $\text{eCO}_2$  (Lu et al., 2016). The largest LAI trend was found in humid regions, which are also important regions contributing to the global averaged LAI trend (Figs. 3 and 4c). Although LAI increased in all climatological regions, the LAI trend in the region where AI showed a decreasing trend was smaller than that in the region where AI showed an increasing trend in the dryland (Fig. 4), consistent with the interannual relationship between LAI and AI being positive in drylands. Humid regions or high-latitude boreal regions are not water-limited but energy-limited (Nemani Ramakrishna et al., 2003), vegetation growth is constrained by temperature and radiation, and short-term precipitation deficiency may result in higher solar radiation and temperature. Less precipitation, cloud cover, and more radiation were favorable for vegetation growth, these conditions ultimately decreased the AI by increasing PET in humid regions (Fig. 8), consistent with the interannual negative relationship between LAI and AI in humid regions (Fig. 6).

The relationship between the AI and LAI decoupled over the study period in drylands and strengthened in humid regions over the same period.

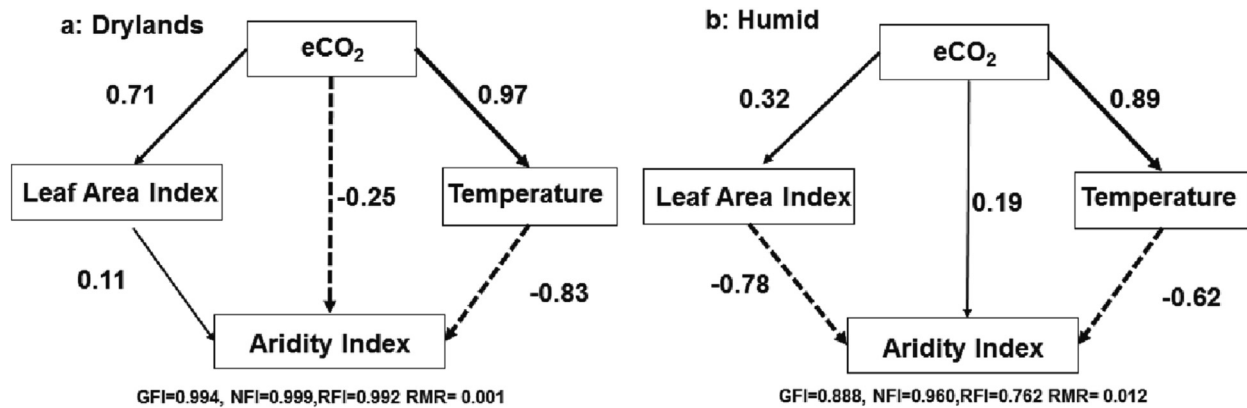


Fig. 9. The structural equation model of leaf area index, aridity index, eCO<sub>2</sub>, temperature in different climatological regions, (a) drylands, and (b) humid regions. The number near the single arrow is the standardized coefficient. GFI: goodness of fit index, NFI: normed fit index, RFI: relative fit index, RMR: root mean square residual.

The greenhouse effect of eCO<sub>2</sub> has contributed to global warming, leading to an increase in PET and a decrease in AI (Figs. 1 and 9). However, warming over land has not been evenly distributed; observations have shown enhanced warming over drylands (Huang et al., 2012; Huang et al., 2017a,b), so the effects of eCO<sub>2</sub> via temperature on the AI in drylands are stronger than those in humid regions (Fig. 9). Our results showed the positive effect of eCO<sub>2</sub> on AI by the LAI in drylands, which may be due to that increase in LAI can increase the amount of transpiring leaf area, leading to an enhanced evapotranspiration (Ukkola et al., 2016; Zhu et al., 2017), which is beneficial for recycling precipitation (Zhang et al., 2022a). Zhang et al. (2022b) also found that the sensitivity of vegetation greenness to precipitation has increased owing to the eCO<sub>2</sub> in drylands. The direct effect of eCO<sub>2</sub> on the AI was negative in drylands and positive in humid region, which was consistent with the ‘wet gets wetter, dry gets drier’ paradigm related to the change in the moisture content of the atmosphere (Wills et al., 2016). The result of the combining direct and indirect effects is that eCO<sub>2</sub> had a negative effect on AI in drylands, while LAI increased owing to the fertilization effect of eCO<sub>2</sub>; thus, LAI and AI were decoupled in drylands. However, the effect of eCO<sub>2</sub> on AI via vegetation was negative in humid regions, where stomatal closure reduced evapotranspiration and increased sensible heat emissions from ecosystems, leading to decreased atmospheric moisture and precipitation (Ukkola et al., 2016; Zhu et al., 2017). Thus, combining the negative effects of eCO<sub>2</sub> on AI through LAI and temperature with the fertilization effect on LAI, the interannual negative relationship between LAI and AI strengthened in humid regions. Our results may be reconciled with previous inconsistent projections about the expansion of drylands in the future. Berg and McColl (2021) did not consider the change in LAI sensitivity to AI in the context of eCO<sub>2</sub>, which resulted in different projections of drylands under climate change scenarios (Huang et al., 2016b).

It is worth noting that previous studies have shown that aridity affects the structure, function, and biodiversity of ecosystems (Berdugo et al., 2020; Shi et al., 2021). As aridity is increasing worldwide (Huang et al., 2016b) and regions where water constraints on vegetation growth are increasing (Jiao et al., 2021), previous studies have indicated that global greening is accompanied by browning under global warming conditions (Kong et al., 2017; Pan et al., 2018). Many studies have also shown that the fertilization effects of eCO<sub>2</sub> are declining (Peñuelas et al., 2017; Wang et al., 2020), indicating that a dryland ecosystem can pass an irreversible tipping point as aridity increases, possibly entering a nonlinear response phase. In this scenario, the mortality risks from drought and heat stress would increase with the transition from a vegetation fertilization-dominated period to one dominated by nutrient and climate constraints on plant growth. Although we revealed the decoupling between AI and LAI in drylands due to eCO<sub>2</sub>, considering the negative effect of eCO<sub>2</sub>, this implies more vulnerability of ecosystems in drylands under global change

and eCO<sub>2</sub>, indicating that desertification remains an issue that requires persistent attention.

Although we investigated the effect of eCO<sub>2</sub> on vegetation sensitive to aridity; however, human activities also influence vegetation growth. Recent studies have shown that China and India dominate the global LAI trend due to land use/change (Chen et al., 2019). This also influences the sensitivity of vegetation to aridity at the local scale. eCO<sub>2</sub> commonly reduces stomatal conductance, which can cause PET to be overestimated in models with unlimited areas (Berg et al., 2016; Milly and Dunne, 2016; Yang et al., 2018, 2019). Although previous studies have shown that the magnitude of the effect of eCO<sub>2</sub> on AI due to decreasing stomatal conductance is small, that was not considered in this study, which may have overestimated the extent of decoupled LAI with AI in drylands. We investigated the effect eCO<sub>2</sub> on vegetation sensitive to aridity based on SEM at a global scale; however, the mechanisms and processes need to be further studied at a regional scale.

## 5. Conclusions

This study investigated the relationship changes between aridity change with vegetation growth in different climatological regions. Over the past three decades, with the exception of arid and semi-arid regions, aridity has increased, and the fertilization effects of eCO<sub>2</sub> have dominated the increasing trend in the global vegetation cover. Interannual changes in P and PET resulted in divergent aridity and vegetation responses in different climatological regions. In drylands, increasing P and decreasing PET produced an increase in the LAI over the study period. In humid regions, this did not necessarily lead to an increase in the LAI. The decoupled relationship between a reduction in aridity and an increase in vegetation cover in drylands was due to the synergistic influence of fertilization and the greenhouse effect of eCO<sub>2</sub>. However, the relationship between the changes in aridity and vegetation growth has been strengthened by eCO<sub>2</sub> in the humid regions over the past three decades. Our results imply that vegetation dynamics prediction should consider spatial aridity changes to avoid uncertainties due to the divergent vegetation response to AI trends in different climatological regions in the future. We also need to pay more attention to the complex effects of eCO<sub>2</sub> on vegetation responses to climate change over different regions to manage vulnerable ecosystems under continued global change.

## CRedit authorship contribution statement

**Guolong Zhang:** Conceptualization, Methodology, Writing – original draft, Writing – review & editing. **Yongli He:** Conceptualization, Methodology, Supervision. **Jianping Huang:** Supervision, Project administration. **Li Fu:** Software, Data curation. **Dongliang Han:** Software, Methodology, Data

curation. **Xiaodan Guan:** Supervision, Data curation. **Beidou Zhang:** Software, Methodology, Data curation.

### Data availability

GIMMS LAI3g could be retrieved from [zhu.zaichun@gmail.com](mailto:zhu.zaichun@gmail.com) on request. Precipitation could be retrieved from <https://psl.noaa.gov/data/gridded/data.prcip.html>. The PET and temperature data could be obtained from <http://crudata.uea.ac.uk/cru/data/hrg/>. The CO<sub>2</sub> data could be retrieved from [https://gml.noaa.gov/aftp/products/trends/co2/co2\\_annmean\\_gl.txt](https://gml.noaa.gov/aftp/products/trends/co2/co2_annmean_gl.txt). AMOS software could be downloaded from <https://www.ibm.com/products/structural-equation-modeling-sem>.

### Declaration of competing interest

The authors declare that they have no known competing financial interests or personal relationships that could have appeared to influence the work reported in this paper.

### Acknowledgements

This work was jointly supported by the National Natural Science Foundation of China (41991231 and 42041004), Youth Science and Technology Fund Project of Gansu (21JR7RA527 and 21JR7RA521) and the Fundamental Research Funds for the Central Universities (lzujbky-2021-kb12, lzujbky-2021-63 and lzujbky-2022-kb09).

### References

Berdugo, M., Delgado-Baquerizo, M., Soliveres, S., Hernández-Clemente, R., Zhao, Y., Gaitán Juan, J., Maestre Fernando, T., 2020. Global ecosystem thresholds driven by aridity. *Science* 367 (6479), 787–790. <https://doi.org/10.1126/science.aay5958>.

Berg, A., McColl, K.A., 2021. No projected global drylands expansion under greenhouse warming. *Nat. Clim. Chang.* 11 (4), 331–337. <https://doi.org/10.1038/s41558-021-01007-8>.

Berg, A., Findell, K., Lintner, B., Giannini, A., Seneviratne, S.I., van den Hurk, B., Milly, P.C.D., 2016. Land-atmosphere feedbacks amplify aridity increase over land under global warming. *Nat. Clim. Chang.* 6, 869. <https://doi.org/10.1038/nclimate3029>.

Brookshire, E.N.J., Weaver, T., 2015. Long-term decline in grassland productivity driven by increasing dryness. *Nat. Commun.* 6 (1), 7148. <https://doi.org/10.1038/ncomms8148>.

Buermann, W., Parida, B., Jung, M., MacDonald, G.M., Tucker, C.J., Reichstein, M., 2014. Recent shift in Eurasian boreal forest greening response may be associated with warmer and drier summers. *Geophys. Res. Lett.* 41 (6), 1995–2002. <https://doi.org/10.1002/2014GL059450>.

Chen, C., Park, T., Wang, X., Piao, S., Xu, B., Chaturvedi, R.K., Myneni, R.B., 2019. China and India lead in greening of the world through land-use management. *Nat. Sustain.* 2 (2), 122–129. <https://doi.org/10.1038/s41893-019-0202-7>.

Cheng, S., Guan, X., Huang, J., Ji, F., Guo, R., 2015. Long-term trend and variability of soil moisture over East Asia. *J. Geophys. Res. Atmos.* 120 (17), 8658–8670. <https://doi.org/10.1002/2015JD023206>.

Conway, T.J., Tans, P.P., Waterman, L.S., Thoning, K.W., Kitzis, D.R., Masarie, K.A., Zhang, N., 1994. Evidence for interannual variability of the carbon cycle from the National Oceanic and Atmospheric Administration/Climate Monitoring and Diagnostics Laboratory Global Air Sampling Network. *J. Geophys. Res. Atmos.* 99 (D11), 22831–22855. <https://doi.org/10.1029/94JD01951>.

Delgado-Baquerizo, M., Maestre, F.T., Gallardo, A., Bowker, M.A., Wallenstein, M.D., Quero, J.L., Zaady, E., 2013. Decoupling of soil nutrient cycles as a function of aridity in global drylands. *Nature* 502 (7473), 672–676. <https://doi.org/10.1038/nature12670>.

Ding, J., Yang, T., Zhao, Y., Liu, D., Wang, X., Yao, Y., Piao, S., 2018. Increasingly important role of atmospheric aridity on Tibetan Alpine grasslands. *Geophys. Res. Lett.* 45 (6), 2852–2859. <https://doi.org/10.1002/2017GL076803>.

Donohue, R.J., Roderick, M.L., McVicar, T.R., Farquhar, G.D., 2013. Impact of CO<sub>2</sub> fertilization on maximum foliage cover across the globe's warm, arid environments. *Geophys. Res. Lett.* 40 (12), 3031–3035. <https://doi.org/10.1002/grl.50563>.

Feng, S., Fu, Q., 2013. Expansion of global drylands under a warming climate. *Atmos. Chem. Phys.* 13 (19), 10081–10094. <https://doi.org/10.5194/acp-13-10081-2013>.

Fensholt, R., Langanke, T., Rasmussen, K., Reenberg, A., Prince, S.D., Tucker, C., Wessels, K., 2012. Greenness in semi-arid areas across the globe 1981–2007 — an Earth Observing Satellite based analysis of trends and drivers. *Remote Sens. Environ.* 121, 144–158. <https://doi.org/10.1016/j.rse.2012.01.017>.

Forzieri, G., Alkama, R., Miralles Diego, G., Cescatti, A., 2017. Satellites reveal contrasting responses of regional climate to the widespread greening of Earth. *Science* 356 (6343), 1180–1184. <https://doi.org/10.1126/science.aal1727>.

Grace, J., 2006. Example analyses. *Structural Equation Modeling and Natural Systems*. Cambridge University Press, Cambridge, pp. 324–349. <https://doi.org/10.1017/CBO9780511617799.015>.

Harris, I., Jones, P.D., Osborn, T.J., Lister, D.H., 2014. Updated high-resolution grids of monthly climatic observations – the CRU TS3.10 dataset. *Int. J. Climatol.* 34 (3), 623–642. <https://doi.org/10.1002/joc.3711>.

He, B., Wang, S., Guo, L., Wu, X., 2019. Aridity change and its correlation with greening over drylands. *Agric. For. Meteorol.* 278, 107663. <https://doi.org/10.1016/j.agrformet.2019.107663>.

Huang, J., Li, Y., Fu, C., Chen, F., Fu, Q., Dai, A., Wang, G., 2017a. Dryland climate change: recent progress and challenges. *Rev. Geophys.* 55 (3), 719–778. <https://doi.org/10.1002/2016RG000550>.

Huang, J., Yu, H., Dai, A., Wei, Y., Kang, L., 2017b. Drylands face potential threat under 2 °C global warming target. *Nat. Clim. Chang.* 7 (6), 417–422. <https://doi.org/10.1038/nclimate3275>.

Huang, N., Shen, Z., Long, S., Wu, M., Shih, H., Zheng, Q., Liu, H., 1998. The empirical mode decomposition and the Hilbert spectrum for nonlinear and non-stationary time series analysis. *Proc. R. Soc. Lond. Ser. A: Math. Phys. Eng. Sci.* 454 (1971), 903–995. <https://doi.org/10.1098/rspa.1998.0193>.

Huang, J., Guan, X., Ji, F., 2012. Enhanced cold-season warming in semi-arid regions. *Atmos. Chem. Phys.* 12 (12), 5391–5398. <https://doi.org/10.5194/acp-12-5391-2012>.

Huang, J., Ji, M., Xie, Y., Wang, S., He, Y., Ran, J., 2016a. Global semi-arid climate change over last 60 years. *Clim. Dyn.* 46 (3), 1131–1150. <https://doi.org/10.1007/s00382-015-2636-8>.

Huang, J., Yu, H., Guan, X., Wang, G., Guo, R., 2016b. Accelerated dryland expansion under climate change. *Nat. Clim. Chang.* 6 (2), 166–171. <https://doi.org/10.1038/nclimate2837>.

Huang, J., Zhang, G., Zhang, Y., Guan, X., Wei, Y., Guo, R., 2020. Global desertification vulnerability to climate change and human activities. *Land Degrad. Dev.* 31 (11), 1380–1391. <https://doi.org/10.1002/ldr.3556>.

IPCC, 2019. In: Shukla, P.R., Skea, J., Buendia, E. Calvo, Masson-Delmotte, V., Pörtner, H.-O., Roberts, D.C., Zhai, P., Slade, R., Connors, S., van Diemen, R., Ferrat, M., Haughey, E., Luz, S., Neogi, S., Pathak, M., Petzold, J., Pereira, J. Portugal, Vyas, P., Huntley, E., Kissick, K., Belkacemi, M., Malley, J. (Eds.), *Climate Change and Land: an IPCC special report on climate change, desertification, land degradation, sustainable land management, food security, and greenhouse gas fluxes in terrestrial ecosystems*.

Ji, F., Wu, Z., Huang, J., Chassignet, E.P., 2014. Evolution of land surface air temperature trend. *Nat. Clim. Chang.* 4 (6), 462–466. <https://doi.org/10.1038/nclimate2223>.

Jiao, W., Wang, L., Smith, W.K., Chang, Q., Wang, H., D'Odorico, P., 2021. Observed increasing water constraint on vegetation growth over the last three decades. *Nat. Commun.* 12 (1), 3777. <https://doi.org/10.1038/s41467-021-24016-9>.

de Jong, R., Verbesselt, J., Schaepman, M.E., de Bruin, S., 2012. Trend changes in global greening and browning: contribution of short-term trends to longer-term change. *Glob. Chang. Biol.* 18 (2), 642–655. <https://doi.org/10.1111/j.1365-2486.2011.02578.x>.

Kharuk, V.I., Ranson, K.J., Oskorbin, P.A., Im, S.T., Dvinskaya, M.L., 2013. Climate induced birch mortality in Trans-Baikal lake region, Siberia. *For. Ecol. Manag.* 289, 385–392. <https://doi.org/10.1016/j.foreco.2012.10.024>.

Kong, D., Zhang, Q., Singh, V.P., Shi, P., 2017. Seasonal vegetation response to climate change in the Northern Hemisphere (1982–2013). *Glob. Planet. Chang.* 148, 1–8. <https://doi.org/10.1016/j.gloplacha.2016.10.020>.

Konings, A.G., Williams, A.P., Gentine, P., 2017. Sensitivity of grassland productivity to aridity controlled by stomatal and xylem regulation. *Nat. Geosci.* 10, 284. <https://doi.org/10.1038/ngeo2903>.

Lu, X., Wang, L., McCabe, M.F., 2016. Elevated CO<sub>2</sub> as a driver of global dryland greening. *Sci. Rep.* 6, 20716. <https://doi.org/10.1038/srep20716>.

Maestre, F.T., Eldridge, D.J., Soliveres, S., Kéfi, S., Delgado-Baquerizo, M., Bowker, M.A., Berdugo, M., 2016. Structure and functioning of dryland ecosystems in a changing world. *Annu. Rev. Ecol. Evol. Syst.* 47 (1), 215–237. <https://doi.org/10.1146/annurev-ecolsys-121415-032311>.

Masarie, K.A., Tans, P.P., 1995. Extension and integration of atmospheric carbon dioxide data into a globally consistent measurement record. *J. Geophys. Res. Atmos.* 100 (D6), 11593–11610. <https://doi.org/10.1029/95JD00859>.

Milly, P.C.D., Dunne, K.A., 2016. Potential evapotranspiration and continental drying. *Nat. Clim. Chang.* 6, 946. <https://doi.org/10.1038/nclimate3046>.

Nemani Ramakrishna, R., Keeling Charles, D., Hashimoto, H., Jolly William, M., Piper Stephen, C., Tucker Compton, J., Running Steven, W., 2003. Climate-driven increases in global terrestrial net primary production from 1982 to 1999. *Science* 300 (5625), 1560–1563. <https://doi.org/10.1126/science.1082750>.

Pan, N., Feng, X., Fu, B., Wang, S., Ji, F., Pan, S., 2018. Increasing global vegetation browning hidden in overall vegetation greening: insights from time-varying trends. *Remote Sens. Environ.* 214, 59–72. <https://doi.org/10.1016/j.rse.2018.05.018>.

Peñuelas, J., Ciais, P., Canadell, J.G., Janssens, I.A., Fernández-Martínez, M., Carnicer, J., Sardans, J., 2017. Shifting from a fertilization-dominated to a warming-dominated period. *Nat. Ecol. Evol.* 1 (10), 1438–1445. <https://doi.org/10.1038/s41559-017-0274-8>.

Piao, S., Wang, X., Park, T., Chen, C., Lian, X., He, Y., Myneni, R.B., 2020. Characteristics, drivers and feedbacks of global greening. *Nat. Rev. Earth Environ.* 1 (1), 14–27. <https://doi.org/10.1038/s43017-019-0001-x>.

Roderick, M.L., Greve, P., Farquhar, G.D., 2015. On the assessment of aridity with changes in atmospheric CO<sub>2</sub>. *Water Resour. Res.* 51 (7), 5450–5463. <https://doi.org/10.1002/2015WR017031>.

Sherwood, S., Fu, Q., 2014. A drier future? *Science* 343 (6172), 737. <https://doi.org/10.1126/science.1247620>.

Shi, H., Tian, H., Lange, S., Yang, J., Pan, S., Fu, B., Reyer Christopher, P.O., 2021. Terrestrial biodiversity threatened by increasing global aridity velocity under high-level warming. *Proc. Natl. Acad. Sci.* 118 (36), e2015552118. <https://doi.org/10.1073/pnas.2015552118>.

Song, X.-P., Hansen, M.C., Stehman, S.V., Potapov, P.V., Tyukavina, A., Vermote, E.F., Townshend, J.R., 2018. Global land change from 1982 to 2016. *Nature* 560 (7720), 639–643. <https://doi.org/10.1038/s41586-018-0411-9>.

- Trolier, M., White, J.W.C., Tans, P.P., Masarie, K.A., Gemery, P.A., 1996. Monitoring the isotopic composition of atmospheric CO<sub>2</sub>: measurements from the NOAA global air sampling network. *J. Geophys. Res. Atmos.* 101 (D20), 25897–25916. <https://doi.org/10.1029/96JD02363>.
- Ukkola, A.M., Prentice, I.C., Keenan, T.F., van Dijk, A.I.J.M., Viney, N.R., Myneni, Ranga B., Bi, J., 2016. Reduced streamflow in water-stressed climates consistent with CO<sub>2</sub> effects on vegetation. *Nat. Clim. Chang.* 6 (1), 75–78. <https://doi.org/10.1038/nclimate2831>.
- Wang, S., Zhang, Y., Ju, W., Chen Jing, M., Ciais, P., Cescatti, A., Peñuelas, J., 2020. Recent global decline of CO<sub>2</sub> fertilization effects on vegetation photosynthesis. *Science* 370 (6522), 1295–1300. <https://doi.org/10.1126/science.abb7772>.
- Wills, R.C., Byrne, M.P., Schneider, T., 2016. Thermodynamic and dynamic controls on changes in the zonally anomalous hydrological cycle. *Geophys. Res. Lett.* 43 (9), 4640–4649. <https://doi.org/10.1002/2016GL068418>.
- Wu, Z., Huang, N.E., 2009. Ensemble empirical mode decomposition: a noise-assisted data analysis method. *Adv. Adapt. Data Anal.* 01 (01), 1–41. <https://doi.org/10.1142/S1793536909000047>.
- Wu, Z., Huang, N.E., Wallace, J.M., Smoliak, B.V., Chen, X., 2011. On the time-varying trend in global-mean surface temperature. *Clim. Dyn.* 37 (3), 759. <https://doi.org/10.1007/s00382-011-1128-8>.
- Yang, Y., Zhang, S., McVicar, T.R., Beck, H.E., Zhang, Y., Liu, B., 2018. Disconnection between trends of atmospheric drying and continental runoff. *Water Resour. Res.* 54 (7), 4700–4713. <https://doi.org/10.1029/2018WR022593>.
- Yang, Y., Roderick, M.L., Zhang, S., McVicar, T.R., Donohue, R.J., 2019. Hydrologic implications of vegetation response to elevated CO<sub>2</sub> in climate projections. *Nat. Clim. Chang.* 9 (1), 44–48. <https://doi.org/10.1038/s41558-018-0361-0>.
- Zhang, J., Wang, S., He, Y., Ren, Y., Huang, J., 2022a. Contribution of the precipitation-recycling process to the wetting trend in Xinjiang, China. *J. Geophys. Res. Atmos.* 127 (11), e2021JD036407. <https://doi.org/10.1029/2021JD036407>.
- Zhang, Y., Gentile, P., Luo, X., Lian, X., Liu, Y., Zhou, S., Keenan, T.F., 2022b. Increasing sensitivity of dryland vegetation greenness to precipitation due to rising atmospheric CO<sub>2</sub>. *Nat. Commun.* 13 (1), 4875. <https://doi.org/10.1038/s41467-022-32631-3>.
- Zhao, M., Running, S.W., 2010. Drought-induced reduction in global terrestrial net primary production from 2000 through 2009. *Science* 329 (5994), 940. <https://doi.org/10.1126/science.1192666>.
- Zhu, Z., Bi, J., Pan, Y., Ganguly, S., Anav, A., Xu, L., Myneni, R.B., 2013. Global data sets of vegetation leaf area index (LAI)3g and fraction of photosynthetically active radiation (FPAR)3g derived from global inventory modeling and mapping studies (GIMMS) normalized difference vegetation index (NDVI3g) for the period 1981 to 2011. *Remote Sens.* 5 (2). <https://doi.org/10.3390/rs5020927>.
- Zhu, Z., Piao, S., Myneni, R.B., Huang, M., Zeng, Z., Canadell, J.G., Zeng, N., 2016. Greening of the Earth and its drivers. *Nat. Clim. Chang.* 6 (8), 791–795. <https://doi.org/10.1038/nclimate3004>.
- Zhu, P., Zhuang, Q., Ciais, P., Welp, L., Li, W., Xin, Q., 2017. Elevated atmospheric CO<sub>2</sub> negatively impacts photosynthesis through radiative forcing and physiology-mediated climate feedback. *Geophys. Res. Lett.* 44 (4), 1956–1963. <https://doi.org/10.1002/2016GL071733>.